2022 19th International Conference on Electrical Engineering, Computing Science and Automatic Control (CCE)
Mexico City, Mexico. November 9-11, 2022

Structural and thermoelectric properties of SnO_2:Bi thin films

D. Trejo-Zamudio
Facultad de Química
UAQ
Santiago de Querétaro, Qro. México
daniel.trejo@uaq.edu.mx

J.G. Quiñones-Galván
Departamento de Física
UDG
Guadalajara, Jalisco, México
jose.quinones@academicos.udg.mx

F.J. de Moure-Flores
Facultad de Química
UAQ
Santiago de Queréretaro, Qro. México
fcomoure@hotmail.com

M.L. Gómez-Herrera
Facultad de Ingeniería
UAQ
Santiago de Queréretaro, Qro. México
lucero.gomez@uaq.mx

J. Santos-Cruz
Facultad de Química
UAQ
Santiago de Querétaro. Qro. México
jsantos@uaq.edu.mx

Abstract*—In this work, the preparation and study of structural and thermoelectric properties of thin films of SnO_2 and SnO_2:Bi are reported. Undoped and doped films were deposited by spray pyrolysis technique at 400 °C. The XRD characterization shows deterioration in the crystalline quality of the samples when the amount of dopant increases. The crystallite size in the samples decreases when the amount of dopant (Bi) increases. Sn^{4+} ion was replaced by Bi^{3+} ion in the lattice of the material. This reduces the concentration of charge carriers but maintains n-type conductivity. The reduction in the concentration of charge carriers and the defects present in the lattice increase the electric resistivity of the material from $2.411x10^{-2}$ Ω·cm to $1.886x10^{2}$ Ω·cm. The Seebeck coefficient increases up to -200 μV/K. However, the sample undoped presented the highest power factor, with a value of 0.51 μW/cm·K². This is because the element Bi creates an insulating effect on the samples both thermally and electrically.

Keywords*—Tin dioxide SnO_2, Bismuth Bi, Thermoelectric material

I. INTRODUCTION

Currently, there are technologies to produce heat, mechanical and electrical energy from renewable and clean energy sources, such as solar, wind, hydro, and bioenergy. However, the energy produced is not used 100 % and statistical results show that more than 60 % of this is wasted throughout the world, especially in form of heat [1].

One way to take advantage of this wasted energy in form of heat is using thermoelectric materials, which are materials with the capacity to convert heat into electricity. In turn, systems that use thermoelectric materials offer the advantages of being friendly to the environment, since they do not produce CO_2 emissions on site, they are small, can work in a wide temperature range, are reliable, and have a long period of life [1, 2].

Currently, there is a great variety of thermoelectric materials, there are materials based on metals, ceramics, polymers, and semiconductors. The variety of materials is due to the search for increasingly efficient materials. The efficiency of thermoelectric material is based on its figure of merit *ZT*. The figure of merit *ZT* is given by the equation:

$$ZT = \propto^2 \sigma T/K \quad (1)$$

where $\propto$ is the Seebeck coefficient, sometimes denoted by *S*, σ is the electrical conductivity and *K* is the thermal conductivity. And the result of the multiplication of $\propto^2$ y σ is known as power factor (PF). A good thermoelectric material has a high electric conductivity and low thermal conductivity.

Semiconductors materials have interesting properties, such as an optimal concentration of charge carriers for thermoelectric applications [3]. For this and other reasons, semiconductors have been investigated for refrigeration and electrical power generation applications since 1950 [2].

Semiconductor materials cover a wide variety of materials, including metal oxides. These, compared to metals, have a good thermoelectric performance, since they have good electrical conductivity and low thermal conductivity. In addition, oxides are friendly to the environment, and they are stable at high temperatures [4].

Among the metal oxides, is tin dioxide (SnO_2). Tin dioxide is considered a member of the transparent conducting oxides (TCO). TCOs include a wide variety of materials that share characteristics that make them attractive for applications in optoelectronic devices, and gas sensors, among others [5]. This particular oxide has been used in solar cells, gas sensors, transparent conductive electrodes, and catalytic supports, due to its chemical advantages and physical properties, such as its mechanical resistance [5, 6].

Tin dioxide has been used in powder form, but for some years it has been of interest to study its nanostructured compounds, such as nanowires, thin films, and nanorods because they present good optical and electrical properties and that could be improved [6]. Its oxide crystallizes in the tetragonal rutile structure (cassiterite) as has been reported in some works [7]. It is generally considered an oxygen deficient n-type semiconductor. It has a bandgap greater than 3 eV, typically ~3.6 eV [6, 8, 9]. It has a concentration of charge carriers (electrons) greater than the order of 10^{-19} and which can be improved by doping [5, 9].

As mentioned, low thermal conductivity in semiconductors is desirable for thermoelectric applications. One way to do this is by creating amorphous or less

978-1-6654-5508-4/22/$31.00 ©2022 IEEE

crystalline quality structures. In this way, the mean free path (MFP) of the phonons is reduced. Some strategies include point defects in the solid structure, nano-scale precipitates, and grain boundaries [1]. As reported, point defects can be achieved by doping or alloying [1]. Doping or heat treatment can also affect the crystallinity of the material. In this case, if a material has a large number of grain boundaries, this can help to have a low thermal conductivity, since each grain boundary allows phonons to scatter [2].

Some recent works have focused on the study of Bi-doped SnO_2 films since they have been observed to exhibit insulating properties. For this reason, this oxide with the same dopant could be used in thermoelectric devices. In the work of Chen et al. (2017), the bismuth-doped tin oxide was used in various proportions to determine the microstructural properties and the transport mechanism found. Bismuth-doped samples showed smaller crystals, a rougher surface, and highly disordered structures compared to undoped ones, indicating crystallinity deterioration with increasing Bi doping concentration [5]. It was found that electrical resistance increased dramatically while electron mobility decreased. Therefore, it is convenient to study the thermoelectric properties of this type of material and determine if it can be used as a thermoelectric material.

In this work, we report the synthesis of thin films of SnO_2 and SnO_2:Bi. This in order to study the effect of Bi on the thermoelectric properties of the oxide. Using a cheaper and faster technique compared to other similar studies. The technique used was spray pyrolysis. The synthesis was carried out at a temperature of 400 ºC. The samples obtained were characterized by X-ray diffraction (XRD), Hall effect, and Seebeck coefficient.

II. METHODOLOGY

A. Preparation of thin films

Thin films of SnO_2 and SnO_2:Bi were obtained by a procedure similar to that described by Choudhury et al. and Djamil et al. [10, 11]. The procedure consisted of two stages, the preparation of precursor solution and the deposit of the thin films by spray pyrolysis.

Glass substrates of 7.5 cm x 2.5 cm were used for the deposition of thin oxide films. The glass substrates were cleaned with soap, treated with chromic acid for 24 hours, and subsequently attacked with a nitric acid solution close to the boiling point for 3 hours. Then, the substrates were rinsed several times with deionized water and stored in a 3:1 mixture of water and ethanol. Before being occupied, the substrates were cut in dimensions of 3.5 x 2.5 cm.

In the first stage, the solution was prepared. The solution started with a mixture of tin chloride dehydrate ($SnCl_2 \cdot 2H_2O$) of Meyer and absolute ethanol (C_2H_5OH) of J.T. Baker. The initial concentration of the solution was 0.2 M. For the preparation of the solution, the required tin chloride was weighed out and placed into a 50 ml beaker. Then, the ethanol was added, and the solution was kept stirring at 1500 rpm. The temperature was raised to 65 °C. The temperature was monitored with the help of a bimetallic thermometer. Upon reaching 60 °C, 5 drops of hydrochloric acid (HCl) of J.T. Baker, were carefully added. The HCl was added to obtain a homogeneous solution [10, 11]. Upon reaching 65 °C, the temperature and stirring were maintained for 2 hours. As the time passed, the solution was allowed to cool while maintaining the agitation until it reached room temperature. To obtain the Bi-doped tin dioxide solution, bismuth nitrate pentahydrate ($Bi(NO_3)_3 \cdot 5H_2O$) of Sigma-Aldrich was used as Bi^{3+} ion precursor. The solution was prepared with the initial concentration of 0.2 M and the bismuth nitrate required was added to obtain concentrations of 0, 0.5, 1.0, 2.0 and 3.0 % atm (Bi/Sn). The samples were labeled as SO_X.XBi, where X.X is the percentage of Bi. The values for X.X were 0.0, 0.5, 1.0, 2.0 and 3.0 respectively.

Once the solution was cold, it was deposited by spray pyrolysis on clean glass substrates. The substrates were placed on the hot plate and the temperature was programmed at 400 °C. Upon reaching the temperature, 5 min were allowed to stabilize the temperature of the hot plate and the substrate. Subsequently, the solution was deposited with the help of an airbrush and N_2 as carrier gas. The deposition angle was 45°, with 30 cm of distance and a deposition flow of 5 ml/min. Total deposition time was 2 min with a total of 10 ml of solution deposited. Table I summarizes the conditions of the deposit. The deposit was constant. Over time, the substrate with the deposited film was allowed to cool to room temperature and the continuity test was performed.

TABLE I. CONDITIONS FOR THE DEPOSIT OF THE THIN FILMS

Control parameter	**Value**
Dimensions of glass substrate	3.5 cm x 2.5 cm
Distance of source to substrate	30 cm
Substrate temperature	400 ºC
Airbrush nozzle opening	Full open
Deposit flow	5 ml/min
Carrier gas	N_2
Gas pressure	1.0 bar
Deposit time	2.0 min
Deposit volume	10.0 ml

B. Characterization techniques

The SO_X.XBi samples were characterized for study as thermoelectric material. X-ray diffractograms, to determine the structure of the materials, were obtained with an Empyrean diffractometer using Cu Kα radiation (λ=1.5406 Å). The thicknesses of the samples were measured with an Alpha-Step D-100 profilometer, KLA Tencor. The electric properties of samples were measured using a Hall Effect Measurement System (ECOPIA HMS-300). Seebeck coefficient of the samples was measured using a system made up of Peltier devices and a Keithley 740 microvoltmeter. Finally, the power factor was obtained by multiplying the electrical conductivity of the material by square of the Seebeck coefficient ($S^2\sigma$).

III. RESULTS AND DISCUSSION

A. XRD characterization

Fig. 1 shows the XRD patterns of the SO_X.XBi samples. The XRD patterns of the samples were compared

with the corresponding card, PDF#41-1445 for SnO_2 (cassiterite). The samples shown only a single phase without diffraction peaks that indicate the presence of impurities or the dopant. The planes that can be observed with greater intensity correspond to (110) at $2\theta \approx 26.611°$, (101) at $2\theta \approx 33.893°$, (200) at $2\theta \approx 37.949°$. The plane (200) is observed with less intensity in the sample SO_0.5Bi with respect to the other samples, perhaps due to the effect of the dopant. Finally, the plane (211) at $2\theta \approx 51.780°$ is observed in all the samples. On the other hand, in the same XRD patterns it can be observed that the full width at half maximum (FWHM) of the peaks increases when the Bi/Sn ratio increase. Also, when the Bi/Sn ratio increase, the samples present loss in the crystalline quality reflected in poorly defined patterns.

Fig. 2 shows a detail on the plane (110). The increase in the width of the peaks is appreciated, which confirms the loss of the crystalline quality. Likewise, the appearance of a signal in the (110) plane is observed in the samples SO_1.0Bi, SO_2.0Bi and SO_3.0Bi, and that increases when the amount of dopant increases. This is due to the defects that the dopant produces in the material lattice. In addition, a slight displacement of the center of the peak to the left is observed for the same reason. This may be due to the difference in the ionic radii of Bi^{3+} (0.96 Å) and Sn^{4+} (0.71 Å) [5]. This difference between ionic radii causes distortions in the material lattice and changes in the distance between atoms [12]. This creates a structure with a lower crystalline quality in the material that reduces the mean free path of the phonons and that is visible in the diffraction patterns. For this reason weakly bonded heavy atoms are often an alternative to lower thermal conductivity and increase the *ZT* [2].

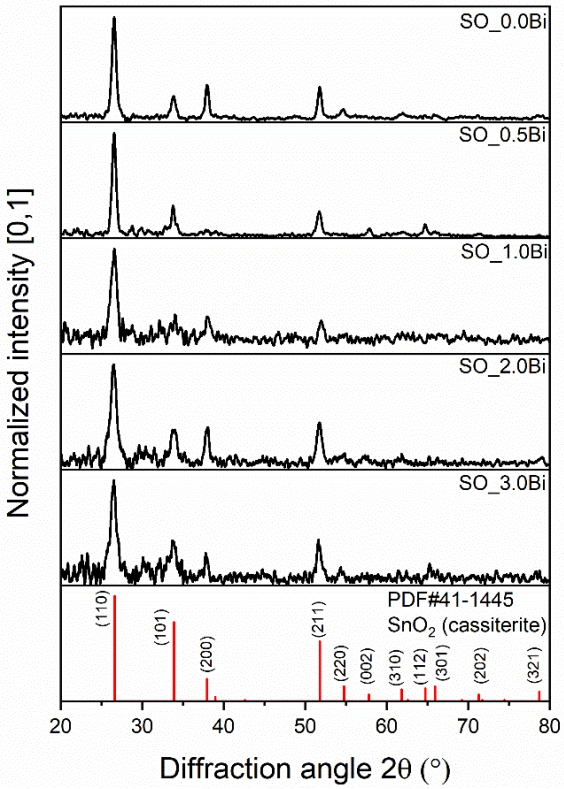

Fig. 1. XRD patterns of the SO_X.XBi samples deposited at 400 °C.

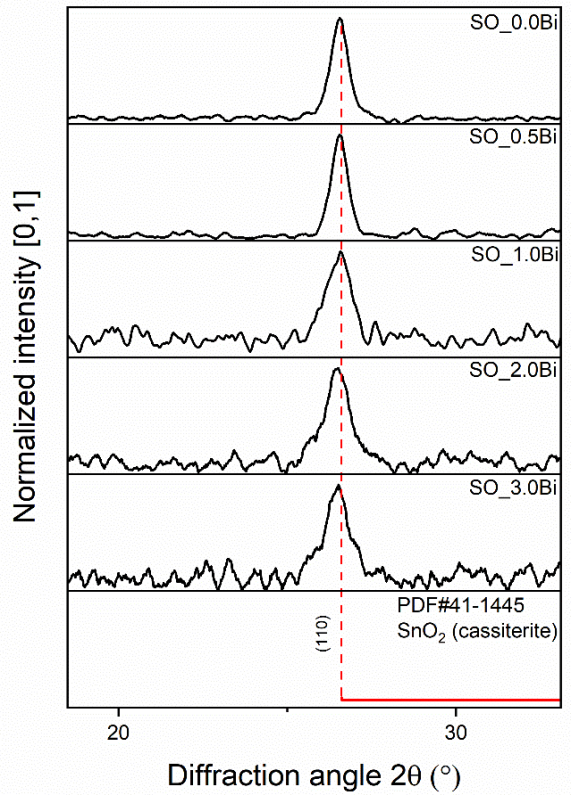

Fig. 2. Detail on the (110) plane region for the SO_X.XBi samples from XRD patterns.

With the diffractograms of Fig. 1, the average size of the crystals (D) was calculated. For this, the Debye-Scherrer equation was employed:

$$D = \frac{0.9\lambda}{\beta cos\theta} \quad (2)$$

Where D is the average of the crystallite size, λ= 1.5406 Å is the Cu K_α radiation, θ is Bragg angle and β is the full width at half maximum (FWHM) of diffraction peak [13]. The crystallite size was calculated from the average of (100) peak and (211) peak. The results are presented in the Table II. The average crystallite size of the undoped sample is 16.51 nm and decrease to 8.16 nm when Bi/Sn ratio increases. This effect is similar to observed in other works when the SnO_2 is doped with elements such as Fe, Cu and Bi [5, 9]. The reason is that impurities introduce point defects that cause changes in stoichiometry due to charge imbalance [9]. In this case, by a heavier atom such as Bi, point defects are produced. These suppress crystallite growth of the material. This is due to mass difference (mass fluctuations and the size and the interatomic coupling forces differences (strain field fluctuations) between the impurity and the hos lattice [1].

TABLE II. CRYSTALLITE SIZE AND THICKNESSES OF SO_X.XBi SAMPLES

Sample	Crystallite size (nm)	Thicknesses (nm)
SO_0.0Bi	16.51	80.0
SO_0.5Bi	12.64	80.0
SO_1.0Bi	9.78	90.0
SO_2.0Bi	8.92	90.0
SO_3.0Bi	8.16	80.0

B. *Electrical characterization*

Table III shows the results of the electrical measurements carried out using the Hall effect. Samples of 1 x1 cm were employed in the van der Pauw configuration. For Hall effect measurement, the thicknesses, obtained by profilometry, were used. In this case, the films had very similar thicknesses, which are reported in Table III. The results for SO_0.0Bi sample (undoped SnO_2) are very close with the reported in the literature. The concentration of charge carriers is lower to that reported (10^{19} to $10^{20}cm^{-3}$) [5, 9,14]. This may be due to technique employed, since very thin films are obtained. In this case, the most direct comparison was made with the work of Joshi et al., since they used a similar technique of deposit. However, they used ITO substrate which could have improved the electrical properties with respect to our work.

TABLE III. ELECTRICAL PROPERTIES OF SO_X.XBi SAMPLES

Sample	**Bulk Concentration *n* (cm^{-3})**	**Mobility μ (cm^2/Vs)**	**Resistivity ρ (Ω·cm)**	**Conductivity σ (1/Ω·cm)**
SO_0.0Bi	$8.703x10^{18}$	75.1	$2.411x10^{-2}$	62.362
SO_0.5Bi	$2.219\ x10^{18}$	3.931	$7.609\ x10^{-2}$	13.090
SO_1.0Bi	$6.388x10^{17}$	0.625	1.294	0.773
SO_2.0Bi	$2.453x10^{17}$	0.348	9.773	0.102
SO_3.0Bi	$8.002x10^{16}$	35.190	$1.886x10^{2}$	$5.873x10^{-3}$
Reference [14]	$9.38\ x10^{19}$	49.6	$1.34\ x10^{-3}$	725

According with the results in the Table III, all the samples present a n-type conductivity. It indicates that the Sn^{4+} ion was replaced by Bi^{3+} ion and there are free electrons if there are oxygen deficiencies. Also, the results indicate that the concentration of charge carriers decrease with increasing Bi/Sn atomic ratio. This is because Sn^{4+} ion was replaced by Bi^{3+} ion, thus reducing the number of electrons available for the conduction process. The reduction of charge carriers produces an increase in electrical resistivity. The sample undoped presented a value of resistivity of $2.411\ x10^{-2}$ Ω·cm similar to $1.5x10^{-2}$ Ω·cm [5] and very close to $1.34x10^{-3}$ [14]. But this value increased up to $1.866x10^{2}$ Ω·cm. This effect has been observed in other works when SnO_2 has been doped with bismuth. This effect has two explanations: the first is the decrease in electron because the substituent ion has one less electron with respect to the substituted ion. The second is that the films doped with Bi may be highly disordered systems, in which electron carriers scattering will increasing greatly due the increased grain boundaries and disorders [5]. Charge carrier mobilities also decrease as defects interact with them, dissipating them and reducing their mobility. Defects include the presence of the doping element and the crystallite boundaries. In addition to that, there are interactions between the charge carriers themselves and the material lattice. However, in the last sample the mobility increases, which may be due to the lower concentration of electrons, which decreases the interaction between them and increases their mobility.

Finally, the Fig. 3 shows the effect in the conductivity of the samples with respect to the concentration of Bi. The conductivity decreases when the concentration of Bi increases. The explanation is the same as in the case of resistivity since conductivity is its inverse. The decrease in the concentration of charge carriers and the grain boundaries affect the conductivity, due to reduction of the mean free path of the electrons.

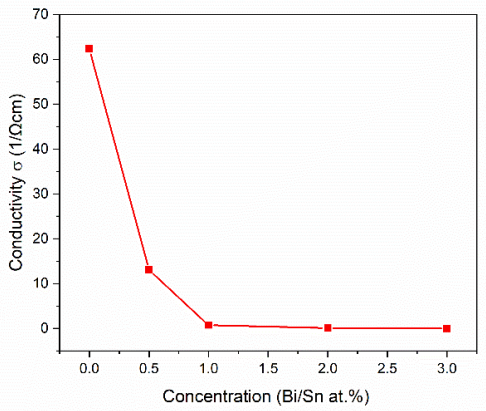

Fig. 3. Effect on electrical conductivity with respect to Bi/Sn concentration.

C. *Seebeck coefficient and power factor*

Table IV shows the Seebeck coefficients and power factors of the samples. The SO_1.0Bi sample has the largest Seebeck coefficient, and the SO_0.0Bi sample has the lowest value. The negative sign is referent the charge carriers in movement, in this case electrons. The relatively high conductivity of the SO_0.0Bi sample allows the Seebeck coefficient to be low. As the concentration of Bi increases, the Seebeck coefficient increases. As can be seen in the Fig. 4, the general trend is to increase the value of Seebeck coefficient. This is because, by decreasing the concentration of charge carriers, the thermal conductivity of the material is affected. Remembering that the total thermal conductivity (k_{tot}) has two contributions: the electronic thermal conductivity (k_{ele}) and the lattice thermal conductivity (k_{lat}) ($k_{tot} = k_{ele} + k_{lat}$) [1]. The first is affected by the decrease in the concentration of charge, while the second is reduced by the grain boundaries of the material. This causes more thermally insulating samples, which generates a greater potential difference between the hot side and the cold side of the material, obtaining a higher Seebeck coefficient. This agrees with the literature, while a material is more insulating, its Seebeck coefficient is higher [3].

Finally, the SO_0.0Bi sample presents the highest power factor of 0.51 μW/cm·K^2. The SO_3.0Bi sample presents the lowest PF value with $1.12x10^{-4}$ μW/cm·K^2. In this case, the best sample with respect to power factor value is the SO_0.0Bi sample. This sample present the highest conductivity and although it has a small Seebeck coefficient, it takes advantage of the potential generated between its hot side and its cold side. In the insulating samples the Seebeck coefficient is higher, due to the difference in potential generated between the hot and cold sides, but the PF is lower because the flow of electrons is bad due to the low electrical conductivity of the material.

TABLE IV. SEEBECK COEFFICIENT AND POWER FACTOR OF SO_X.XBi SAMPLES

Sample	Seebeck coefficient S (μV/K)	Power factor $S^2\sigma$ (μW/cm·K²)
SO_0.0Bi	-91.0	0.51
SO_0.5Bi	-139.0	0.25
SO_1.0Bi	-200.0	$3.09x10^{-2}$
SO_2.0Bi	-142.0	$2.06x10^{-3}$
SO_3.0Bi	-138.0	$1.12x10^{-4}$

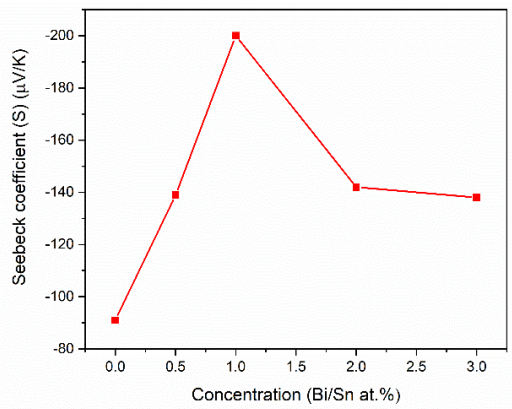

Fig. 4. Effect on the Seebeck coefficient with respect to the concentration of Bi/Sn.

IV. CONCLUSIONS

Thin films of SnO_2 and SnO_2:Bi were obtained by spray pyrolysis technique with a substrate temperature of 400 °C. The samples doped with Bi have smaller crystallites with respect to the undoped sample. The substitution of Sn^{4+} ion by Bi^{3+} ion decrease the concentration of charge carriers and increase the electrical resistivity. These conditions favor the improvement of the Seebeck coefficient, by having a more insulating material with respect to undoped material. However, the electrical conductivity decreases, which affects the thermoelectric properties of the films. It is for this reason that the undoped film has the highest PF value. Thus, the incorporation of Bi affects the electrical and thermal properties of the material, so the doped material is not suitable for thermoelectric applications. However, the quantification of thermal conductivity is necessary to determine the *ZT* values and check if it also decreases as the power factor value.

AKNOWLEDGMENT

The authors acknowledgment the support from CONACYT provided to the student Daniel Trejo Zamudio for his scholarship in postgraduate studies and UAQ (FQST 2021, JSC for partial financial support). We acknowledge the technical support of Instituto de Energías Renovables, UNAM for the Seebeck coefficient measurements.

V. REFERENCES

[1] X. Zhang y L. Zhao, "Thermoelectric materials: Energy conversion between heat and electricity", *J. Mater.*, vol. 1, núm. 2, pp. 92–105, 2015, doi: 10.1016/j.jmat.2015.01.001.

[2] M. Hamid, Elsheikh *et al.*, "A review on thermoelectric renewable energy: Principle parameters that affect their performance", *Renew. Sustain. Energy Rev.*, vol. 30, pp. 337–355, 2014, doi: 10.1016/j.rser.2013.10.027.

[3] Linseis, "El coeficiente de Seebeck", 2021. https://www.linseis.com/es/propiedades/coeficiente-de-seebeck/.

[4] Y. F. Wang, K. H. Lee, H. Ohta, y K. Koumoto, "Fabrication and thermoelectric properties of heavil y rare-earth metal-doped SrO($SrTiO_3$)n (n=1,2) ceramics.", *Ceram Int*, vol. 34, pp. 849–52, 2008.

[5] C. Z. Chen, S. W. Zhu, W. Q. Zhang, Y. Li, y C. B. Cai, "Microstructural properties and carrier transport mechanism in Bi-doped nanocrystalline SnO_2 thin films", *Results Phys.*, vol. 7, pp. 2588–2593, 2017, doi: 10.1016/j.rinp.2017.07.039.

[6] Z. Chen *et al.*, "Recent advances in tin dioxide materials: Some developments in thin films, nanowires, and nanorods", *Chem. Rev.*, vol. 114, núm. 15, pp. 7442–7486, 2014, doi: 10.1021/cr4007335.

[7] H. Köse, Ş. Karaal, A. O. Aydin, y H. Akbulut, "Structural properties of size-controlled SnO_2 nanopowders produced by sol-gel method", *Mater. Sci. Semicond. Process.*, vol. 38, pp. 404–412, 2015, doi: 10.1016/j.mssp.2015.03.028.

[8] A. Ammari, B. Bellal, N. Zebbar, B. Benrabah, y M. Trari, "Thermal-frequency dependence study of the sub-band localized states effect in Sb-doped SnO_2 based sol-gel thin films", *Thin Solid Films*, vol. 632, pp. 66–72, 2017, doi: 10.1016/j.tsf.2017.02.060.

[9] M. A. Batal, G. Nashed, y F. H. Jneed, "Conductivity and thermoelectric properties of nanostructure tin oxide thin films", *J. Assoc. Arab Univ. Basic Appl. Sci.*, vol. 15, núm. 1, pp. 15–20, 2013, doi: 10.1016/j.jaubas.2012.09.005.

[10] S. P. Choudhury, S. D. Gunjal, N. Kumari, K. D. Diwate, K. C. Mohite, y A. Bhattacharjee, "Facile synthesis of SnO_2 thin film by spray pyrolysis technique and investigation of the structural, optical and electrical properties", *Mater. Today Proc.*, vol. 3, núm. 6, pp. 1609–1619, 2016, doi: 10.1016/j.matpr.2016.04.050.

[11] R. Djamil, K. Aicha, A. Souifi, y D. Fayçal, "Effect of annealing time on the performance of tin oxide thin films ultraviolet photodetectors", *Thin Solid Films*, vol. 623, pp. 1–7, 2017, doi: 10.1016/j.tsf.2016.12.035.

[12] C. Nuñez, A. Roca, y J. Jorba, *Comportamiento mecánico de los materiales. Volumen I. Conceptos fundamentales*, Segunda Ed. Edicions Universitat Barcelona, 2012.

[13] R. E. Dinnebier y S. J. L. Billinge, *Powder Diffraction, Theory and Practice*. RSC Publishing, 2008.

[14] B. N. Joshi, H. Yoon, y S. S. Yoon, "Structural, optical and electrical properties of tin oxide thin films by electrostatic spray deposition", *J. Electrostat.*, vol. 71, pp. 48–52, 2013.